Ain Shams Engineering Journal xxx (xxxx) xxx

Contents lists available at ScienceDirect

Ain Shams Engineering Journal

journal homepage: www.sciencedirect.com

Computational results of convective heat transfer for fractionalized Brinkman type tri-hybrid nanofluid with ramped temperature and non-local kernel

Muhammad Amir [a], Qasim Ali [a], Ali Raza [a,b], M.Y. Almusawa [c], Waleed Hamali [c], Ali Hasan Ali [d,e,f,*]

[a] Department of Mathematics, University of Engineering and Technology, Lahore 54890, Pakistan
[b] Department of Mathematics, Minhaj University, Lahore 54770, Pakistan
[c] Department of Mathematics, Faculty of Science, Jazan University, Jazan, Saudi Arabia
[d] Institute of Mathematics, University of Debrecen, Pf. 400, H-4002 Debrecen, Hungary
[e] College of Engineering Technology, National University of Science and Technology, 64001 Dhi Qar, Iraq
[f] Technical Engineering College, Al-Ayen University, 64001 Dhi Qar, Iraq

ARTICLE INFO

Keywords:
Heat transfer
AB time-fractional derivative
Brinkman type fluid
Tri-hybrid nanofluid
Ramped temperature
Laplace transform

ABSTRACT

Engineers have recently become attracted to electrically conducting nanofluids (NFs) due to various applications in several applied science and engineering disciplines. They have been employed in magnetic refrigeration, cancer treatment (hyperthermia), medicine, and magnetic resonance imaging, among other things. Considering the importance of electrically conducting NFs, in this article, we have proposed a fractionalized MHD (Magnetohydrodynamics) and thermal transmission of a Brinkman-type tri-hybrid nanofluid over an infinite plate saturated through a porous medium with generalized velocity and ramped conditions. For the solution of the governed fractional model, we have utilized a recent definition of fractional derivatives, known as Atangana-Baleanu (AB) fractional derivative and Laplace transformation. The computational results are exhibited for tri-hybrid (TiO_2-Al_2O_3-CuO/H_2O) NF and described through graphical diagrams and tables to discover the physics of numerous relevant flow parameters on temperature and velocity profiles. It is detected that both thermal transmission and momentum profile for tri-hybrid NF is a better technique as compared to hybrid NF and NF for both graphical and numerical comparisons.

1. Introduction

Various natural fluids reserve very low TC (thermal conductivity) for thermal transfer, which is observed as an essential wall in the expansion of heat flow schemes. Manufacturing several components and devices utilized in engineering and industrial applications has progressed suggestively in the contemporary world. For instance, in manufacturing, numerous implements started to raise their temperature with time because of the confrontation of electricity. Due to the electric conflict, such devices' thermal-transferring competence declined, resulting in a mechanical deficiency. Heat excess from several instruments and mechanisms is compulsory to decrease the danger of mechanical defects. Consequently, manufacturers use liquids like air, water, and lubricants to succeed in appropriate heat transportation. However, such common fluids are never used in the production process. Researchers investigated various approaches for retaining fluid mobility and heat transference inside the building border to achieve these goals. Because of their lower TC, nanoparticles (NPs) may be incorporated into various conventional fluids. Moreover, the characteristics of NFs may be formed for a specific request if needed. The idea to add NPs was presented by Choi et al. [1]. The flow of NPs on a wedge in a porous media by employing a convective fluid movement comprised the impacts of numerous particle morphologies by Ellahi et al. [2] in their work. Considering Brownian motion, an electrically conductive thermal transmission for buoyancy and NF movement through a rigid surface and supposing two characters was examined in [3,4]. Using a cylindrically designed annulus, the convection of thermal transmission for NPs was modeled numerically and discussed in [5]. Gourari et al. [6] investigated convective flow in coaxal inclined tubes. MebarekOudina [7] studied convective thermal

* Corresponding author.
E-mail addresses: aliraza.math@mul.edu.pk (A. Raza), malmusawi@jazanu.edu.sa (M.Y. Almusawa), wahamali@jazanu.edu.sa (W. Hamali), ali.hasan@science.unideb.hu (A.H. Ali).

https://doi.org/10.1016/j.asej.2023.102576
Received 9 April 2023; Received in revised form 3 June 2023; Accepted 4 November 2023

Nomenclature

β_0	Brinkman parameter , [−]
B_o	Magnetic field strength, $[Kg/s^2]$
g	Gravitational acceleration, $[LT^{-2}]$
u	Velocity of fluid, $[LT^{-1}]$
T	The temperature of the fluid , $[K]$
K	Permeability of porous medium , $[L]$
T_W	The temperature of the fluid on the plate, **[K]**
U_o	Constant velocity, $[LT^{-1}]$
$g(t)$	The velocity of the plate, $[LT^{-1}]$
T_∞	The temperature of fluid away from the plate, [K]
β_1	Dimensionless Brinkman parameter , [−]
M	Dimensionless magnetic parameter , [−]
Gr	Grashof number , [−]
Pr	Prandtl number , [−]
K_1	Dimensionless permeability parameter , [−]
q	Laplace transformed variable , [−]
ξ	Atangana-Baleanu fractional derivative parameter , [−]

Abbreviations

NFs	Nanofluids
HNFs	Hybrid Nanofluids
NPs	Nanoparticles
TC	Thermal Conductivity
MHD	Magnetohydrodynamics
AB	Atangana-Balenau time-fractional derivative

transfer with the titania NF using a variety of base liquids. Raza et al. [8] investigated an MHD model with varied NPs across a channel by evaluating the effects of various shapes. In their work, they studied the impact of NPs on the flow of the MHD model. [9] examined the domain of MHD, while [10] considered the numerical behavior of an MHD HNF in a permeable stretching medium. Chamkha et al. [11] reflected the free convection of MHD NF in addition to the impact of thermal radiation. By employing the Duan Rach technique, for turbine freezing submissions, the equations for thermal transmission of a non-Newtonian fluid were done in [12]. Veera Krishna [13] explored the thermal communication of NFs flow with the MHD effect. The MHD effect of HNFs was discussed in [14] numerically. Krishna et al. [15] have newly observed an MHD Casson HNF flow across an enormous enhanced perpendicular porous surface. Ramadhan et al. [14] studied water-ethylene-based trinary hybrid nanofluids' thermal stability and thermal conductivity. They analyzed different nanoparticles' thermal conductivity and concluded some preliminary results. Muzaidi et al. [15] have investigated the solution of *CuO/TiO2/SiO2*-based ternary-nanofluid and analyzed its solar thermal applications. The thermal applications and the stability of ternary hybrid nanofluid moving through a Darcy–Forchheimer porous medium was examined by Gul et al. [16]. A tri-hybrid NF is a novel concept in a research domain and presents a reasonable thermal transmission rate than hybrid nanofluid and nanofluid. Further investigations regarding the ternary hybrid nanofluid can be seen in the [17–20].

Non-Newtonian fluids have their place in that category of fluids where the flow profile, i.e., the connection of shear stress and deformation rate, is non-linear. Milk, Blood, toothpaste, and paint are examples of non-Newtonian fluids. Non-Newtonian fluids are used in a variety of everyday applications. Non-Newtonian fluids have uses such as drag reduction agents, printing technologies, dampening and braking devices, personal protection equipment, and culinary ingredients. Non-Newtonian fluids are also used to increase printing technology quality. These non-Newtonian fluids increase ink viscosity and flow behavior, resulting in a more transparent printing experience. Damper and braking systems also use non-Newtonian fluids. The magnetorheological fluid in shocks and rotors is modified dimethyl silicone oil. Diverse non-Newtonian fluids reveal changed rheological structures, for instance, shear thickening, shear thinning, etc. Due to their composite shape, we don't find any single equations that may reveal non-Newtonian fluids' physical and mathematical appearance. Nonetheless, these fluids are healthily respected in manufacturing, technology, and science due to their varied submissions on particular grounds, like the engineering of damping strategies, drag-declining representatives, printing skills, mechanical phenomena, medicines, etc. [21–23]. Numerous models in the literature designate non-Newtonian fluids, and Brinkman fluid is one of them from this class of fluids. In 1856, Darcy [24] anticipated a model that contains fluid motion with a small porous area. Nevertheless, Darcy's model is unreliable for fluid passing over a sizeable porous region. Therefore, Brinkmann [25,26] proposed a fluid model in which fluid moves over a sizeable porous zone. Brinkmann fluid explains those viscous fluids that pass over the high porous zone. Firstly, Brinkman [27] examined the viscid force fashioned through the compressed group of particles. Brinkman [26] stretched the prior research work of viscid fluids by extending the particles' swarm and containing Darcy's model as the unique case. Several technical and manufacturing flows comprise Brinkman flow, like tank manufacturing, groundwater hydrology, soil science, and chemical engineering [28,29]. Gorla et al. [30] discussed the natural convection flow and exposed the parametric significances of hydro-thermal disparities. Lin and Payen [31] examined the Brinkman model's mechanical constancy.

Fractional calculus (FC) has engaged a significant place in the ground of research owing to its vigorous characteristics as a memory effect. Because of such positivity, the FC is considered everywhere for two aspects, i.e., non-singularity as well as non-locality dominant in kernels of fractional derivatives. From the early phase of the fractional derivatives, Caputo and Riemann–Liouville fractional approaches were constructed on a singular kernel, which can't cover all the memory influences in viscoelasticity and viscoplasticity. To handle this situation of the particular kernel, Caputo and Fabrizio anticipated the fractional operator involving non-singular and exponential kernel, i.e., Caputo–Fabrizio fractional derivative. Caputo–Fabrizio demonstrated a very operative fractional operator. Nevertheless, it does not have locality characteristics in the kernel. Because of non-locality in the kernel, the fractional derivative is only composed of memory influences at scattering themes, nonetheless, it may not contain the entire domain for finding memory effects. Later, Atangana and Baleanu familiarized a fractional operator involving non-local and non-singular Mittag–Leffler kernel. This fractional derivative can cover memory effects at individual sprinkling points [32–35]. However, for simplicity of this paper, the recent work of fractional technique with evaluations, exact and numerical solutions, and flow models are referenced in more studies [36–39].

This paper aims to examine the non-Newtonian fractionalized MHD flow and thermal transmission of a Brinkman-type tri-hybrid NF over an infinite plate saturated in a porous medium along with generalized velocity and ramped temperature. First, the Brinkman Type tri-hybrid NF model is formulated in the AB fractional domain. A tri-hybrid NF is a new concept in the research field, presenting a better thermal transmission rate than HNF and NF. Finally, to see the physical features of the problem, the various disparities and differential parametric investigation are offered with graphical diagrams.

2. Mathematical modeling

Suppose the unsteady incompressible flow of a tri-hybrid nanofluid

coupled with heat transfer over an infinite plate saturated in a porous medium with ramped heating temperature. The fluid is assumed to be electrically conducting; hence, an external magnetic field is utilized generally in the flow direction. It is supposed that initially ($t \leq 0$), the system was on relaxation at ambient temperature. However, after a short interval of time, the plate starts moving with variable velocity $u_0 g(t)$ where u_0 is the amplitude of movement, and in addition, the fluid temperature at the plate advances from T_∞ to $T_\infty + (T_W - T_\infty)t/t_0$ when $0 < t < t_0$ or T_W when $t > t_0$. Convection takes place because of the temperature gradient and the plate's movement. So, fluid starts motion in the x-direction, as shown in Fig. 1.

The governing equations of Brinkman-type tri-hybrid nanofluid [40] under the Boussinesq approximation are [41,42]

$$\frac{\partial u_{(y,t)}}{\partial t} + \beta_0 u_{(y,t)} = \frac{\mu_{thnf}}{\rho_{thnf}} \frac{\partial^2 u_{(y,t)}}{\partial y^2} - \left(\frac{\sigma_{thnf}}{\rho_{thnf}} B_o^2 + \frac{\nu_{thnf}}{K} \right) u_{(y,t)} + g(\beta_t)_{thnf} \left(T_{(y,t)} - T_\infty \right) \tag{1}$$

$$\left(\rho C_p\right)_{thnf} \frac{\partial T_{(y,t)}}{\partial t} = K_{nf} \frac{\partial^2 T_{(y,t)}}{\partial y^2}, \tag{2}$$

where ρ_{thnf}, μ_{thnf}, υ_{thnf}, σ_{thnf}, $(\beta_t)_{thnf}$, $(\rho C_P)_{thnf}$ and K_{thnf} are density, viscosity, dynamic viscosity, electrical conductivity, thermal extension coefficient, heat capacitance, and TC of tri-hybrid NF correspondingly and defined by [43,44],

$$\mu_{thnf} = \frac{\mu_f}{\left(1 - \phi_{thnf}\right)^{2.5}}, \rho_{thnf} = \rho_f \left(1 - \phi_{thnf}\right) + \phi_1 \rho_{s1} + \phi_2 \rho_{s2} + \phi_3 \rho_{s3},$$

$$\sigma_{thnf} = \sigma_f \left(\frac{\sigma_{s1}\phi_1 + \sigma_{s2}\phi_2 + \sigma_{s3}\phi_3 + 2\sigma_f \phi_{thnf} + 2\phi_{thnf}\left(\sigma_{s1}\phi_1 + \sigma_{s2}\phi_2 + \sigma_{s3}\phi_3 - \sigma_f \phi_{thnf}\right)}{\sigma_{s1}\phi_1 + \sigma_{s2}\phi_2 + \sigma_{s3}\phi_3 + 2\sigma_f \phi_{thnf} - \phi_{thnf}\left(\sigma_{s1}\phi_1 + \sigma_{s2}\phi_2 + \sigma_{s3}\phi_3 - \sigma_f \phi_{thnf}\right)} \right),$$

$$K_{thnf} = K_f \left(\frac{K_{s1}\phi_1 + K_{s2}\phi_2 + K_{s3}\phi_3 + 2K_f \phi_{thnf} + 2\phi_{thnf}\left(K_{s1}\phi_1 + K_{s2}\phi_2 + K_{s3}\phi_3 - K_f \phi_{thnf}\right)}{K_{s1}\phi_1 + K_{s2}\phi_2 + K_{s3}\phi_3 + 2K_f \phi_{thnf} - \phi_{thnf}\left(K_{s1}\phi_1 + K_{s2}\phi_2 + K_{s3}\phi_3 - K_f \phi_{thnf}\right)} \right),$$

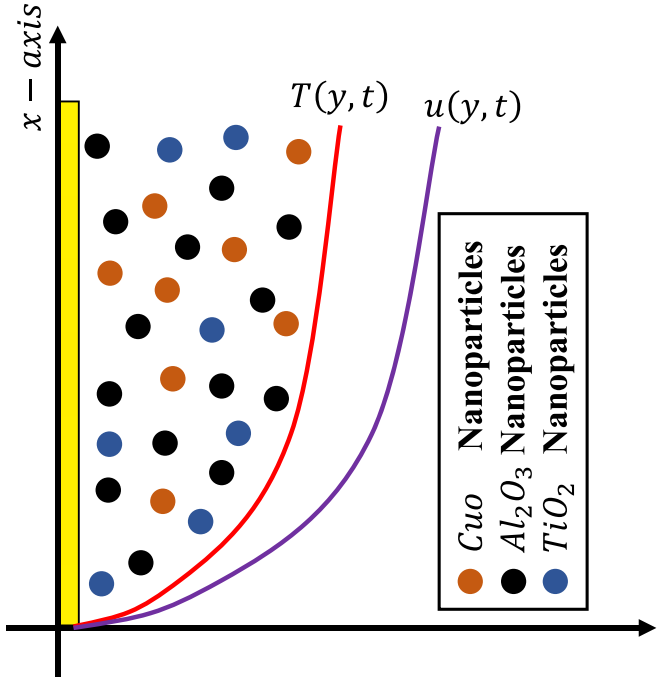

Fig. 1. Physical flow.

$$\phi_{thnf} = \phi_1 + \phi_2 + \phi_3.$$

Eqs. (1) and (2) have the following initial and boundary conditions:

$$u_{(y,0)} = 0, T_{(y,0)} = T_\infty; \forall y \geq 0 \tag{3}$$

$$u_{(0,t)} = U_o g(t), s$$

$$T_{(y,t)} = \begin{cases} T_\infty + (T_w - T_\infty)\dfrac{t}{t_o}, if 0 < t \leq t_o \\ T_w, if t > t_o \end{cases}, \tag{4}$$

$$u_{(y,t)} \to 0, T_{(y,t)} \to T_\infty, as y \to \infty, t > 0. \tag{5}$$

The subscripts hnf, f, and s are denoted as tri-hybrid nanofluid, base fluid, as well as solid nanoparticles (see Fig. 2).

The following non-dimensional parameters have been employed for dimensional analysis.

$$u^* = \frac{u}{U_o}, y_1 = \frac{U_o}{\upsilon_f} y, t_1 = \frac{t}{t_o}, t_o = \frac{\upsilon_f}{U_o^2}, T_1 = \frac{T_{(y,t)} - T_\infty}{T_w - T_\infty} \tag{6}$$

By discarding the steric notation, we get the following dimensionless system after depersonalization:

$$\frac{\partial u_{(y_1,t_1)}}{\partial t_1} + \beta_1 u_{(y_1,t_1)} = \Lambda_1 \frac{\partial^2 u_{(y_1,t_1)}}{\partial y_1^2} - \left(\Lambda_2 M + \frac{\Lambda_1}{K_2} \right) u_{(y_1,t_1)} + \mathrm{Gr}_1 T_{1(y_1,t_1)} \tag{7}$$

$$\mathrm{Pr}_1 \frac{\partial T_{1(y_1,t_1)}}{\partial t_1} = \frac{\partial^2 T_{1(y_1,t_1)}}{\partial y_1^2}, \tag{8}$$

$$u_{(y_1,0)} = 0, T_{1(y_1,0)} = 0; \forall y \geq 0 \tag{9}$$

$$u_{(0,t_1)} = g(t_1), T_{(0,t_1)} = \begin{cases} t_1, if 0 < t_1 \leq 1 \\ 1, if t_1 > 1 \end{cases} \tag{10}$$

$$w_{(y_1,t_1)} \to 0, T_{(y_1,t_1)} \to 0; y \to \infty, t > 0 \tag{11}$$

where

$$b_1 = (1 - \phi_1 - \phi_2 - \phi_3) + \phi_1 \frac{\rho_{s1}}{\rho_f} + \phi_2 \frac{\rho_{s2}}{\rho_f} + \phi_3 \frac{\rho_{s3}}{\rho_f}, b_2 = \frac{1}{(1 - \phi_1 - \phi_2 - \phi_3)^{2.5}},$$

$$b_3 = \frac{\sigma_{s1}\phi_1 + \sigma_{s2}\phi_2 + \sigma_{s3}\phi_3 + 2\sigma_f \phi_{thnf} + 2\phi_{thnf}\left(\sigma_{s1}\phi_1 + \sigma_{s2}\phi_2 + \sigma_{s3}\phi_3 - \sigma_f \phi_{thnf}\right)}{\sigma_{s1}\phi_1 + \sigma_{s2}\phi_2 + \sigma_{s3}\phi_3 + 2\sigma_f \phi_{thnf} - \phi_{thnf}\left(\sigma_{s1}\phi_1 + \sigma_{s2}\phi_2 + \sigma_{s3}\phi_3 - \sigma_f \phi_{thnf}\right)},$$

$$b_4 = (1-\phi_1-\phi_2-\phi_3)+\phi_1\frac{(\beta_1)_{s1}}{(\beta_1)_f}+\phi_2\frac{(\beta_1)_{s2}}{(\beta_1)_f}+\phi_3\frac{(\beta_1)_{s3}}{(\beta_1)_f}, b_5 = (1-\phi_1-\phi_2-\phi_3)+\phi_1\frac{(\rho C_p)_{s1}}{(\rho C_p)_f}+\phi_2\frac{(\rho C_p)_{s2}}{(\rho C_p)_f}+\phi_3\frac{(\rho C_p)_{s3}}{(\rho C_p)_f}, b_6$$
$$= \frac{K_{s1}\phi_1+K_{s2}\phi_2+K_{s3}\phi_3+2K_f\phi_{thnf}+2\phi_{thnf}\left(K_{s1}\phi_1+K_{s2}\phi_2+K_{s3}\phi_3-K_f\phi_{thnf}\right)}{K_{s1}\phi_1+K_{s2}\phi_2+K_{s3}\phi_3+2K_f\phi_{thnf}-\phi_{thnf}\left(K_{s1}\phi_1+K_{s2}\phi_2+K_{s3}\phi_3-K_f\phi_{thnf}\right)}, Pr = \left(\frac{\mu C_p}{\kappa}\right)_f, M = \frac{\sigma_f B_0{}^2 \upsilon_f}{\rho_f U_0{}^2}, \frac{1}{K_2} = \frac{\upsilon_f{}^2}{U_0{}^2 K}, Gr = \frac{g(\beta_t)_f \upsilon_f (T_w - T_\infty)}{U_o^3}, \beta_1$$
$$= \frac{\beta_0 \upsilon_f}{U_o^2}, \Lambda_1 = \frac{b_2}{b_1}, \Lambda_2 = \frac{b_3}{b_1}, Gr_1 = Grb_4, \mathrm{Pr}_1 = Pr\frac{b_5}{b_6}.$$

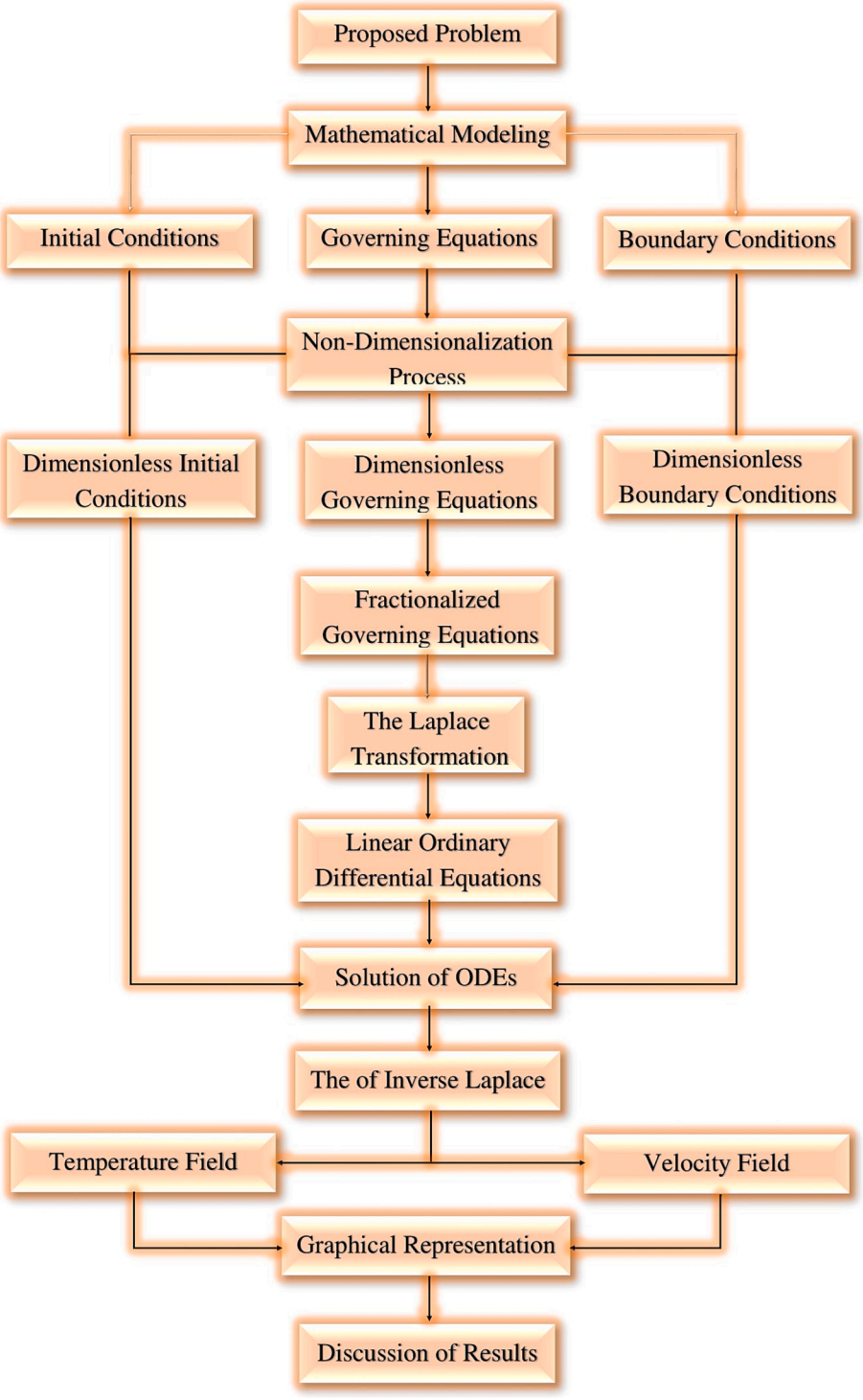

Fig. 2. Flow chart of the considered problem.

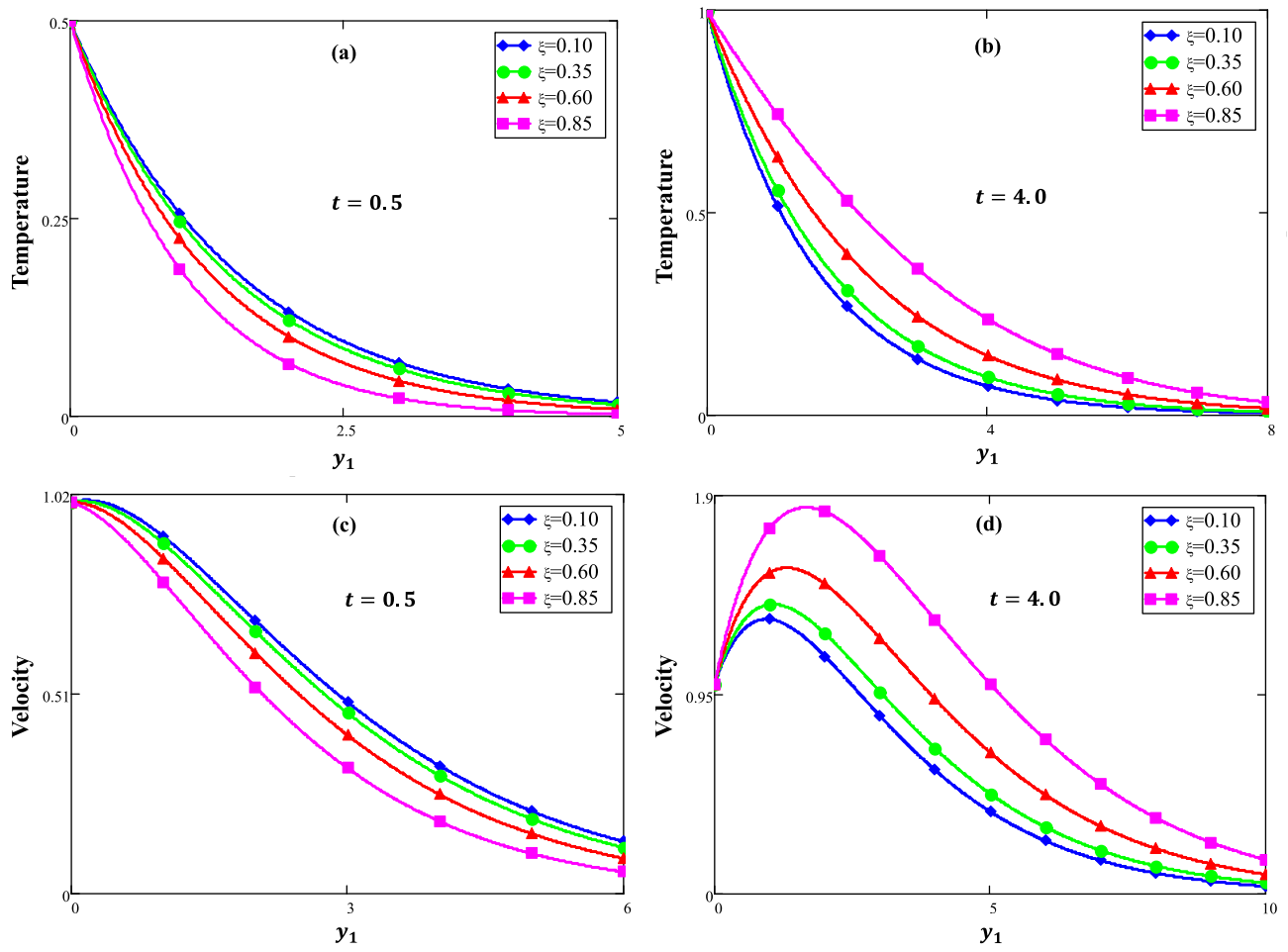

Fig. 3. Significance of fractional parameter ξ on the temperature field and velocity profile.

Formulation of Fractional Model

Here, the ordinary derivatives in the dimensionless equations are replaced with the recently introduced AB derivative operator as follows

$$ {}^{AB}D_{t_1}^{\xi} u_{(y_1,t_1)} + \beta_1 u_{(y_1,t_1)} = \Lambda_1 \frac{\partial^2 u_{(y_1,t_1)}}{\partial y_1^2} - \left(\Lambda_2 M + \frac{\Lambda_1}{K_2}\right) u_{(y_1,t_1)} + \mathrm{Gr}_1 T_{1(y_1,t_1)} \tag{12} $$

$$ Pr_1 {}^{AB}D_{t_1}^{\xi} T_{1(y_1,t_1)} = \frac{\partial^2 T_{1(y_1,t_1)}}{\partial y_1^2}, \tag{13} $$

Here AB derivative is defined for the function $\Pi(y_1,t_1)$ by

$$ {}^{AB}\mathfrak{D}_{t_1}^{\xi}\ \Pi(y_1,t_1) = \frac{N(\xi)}{1-\xi}\int_0^{t_1} E_{\xi}\left[\frac{\xi(t-z)^{\xi}}{1-\xi}\right]\Pi'(y_1,t_1)dt_1;\ 0<\xi<1, \tag{14} $$

where $N(\xi)$ is the normalization function and here we have $N(0) = N(1) = 1$ and $\xi \in (0,1)$ and $E_{\xi}(z)$ is a Mittage-Leffler function demarcated as

$$ E_{\xi}(z) = \sum_{i=0}^{\infty} \frac{z^{\xi}}{\Gamma(i\xi+1)};\ 0<\xi<1,\ z\in\mathbb{C}. \tag{15} $$

The Laplace transform of the AB operator is

$$ \mathscr{L}\left\{ {}^{AB}\mathfrak{D}_t^{\xi}\Pi(y_1,t_1)\right\} = \frac{q^{\xi}\mathscr{L}[\Pi(y_1,t_1)] - q^{\xi-1}\Pi(y_1,0)}{(1-\xi)q^{\xi}+\xi} \tag{16} $$

With

$$ \lim_{\xi\to 1} {}^{AB}\mathfrak{D}_{t_1}^{\xi}\Pi(y_1,t_1) = \frac{\partial\Pi(y_1,t_1)}{\partial t_1} \tag{17} $$

3. Solution of the problem

3.1. Solution for the energy equation

Applying the Laplace transform to Eq. (13) and with conditions $(9)_2$-$(11)_2$, we obtain

$$ \overline{T}_{1(y_1,q)} = c_1 e^{y_1\sqrt{\frac{\mathrm{Pr}_1 q^{\xi}}{(1-\xi)q^{\xi}+\xi}}} + c_2 e^{-y_1\sqrt{\frac{\mathrm{Pr}_1 q^{\xi}}{(1-\xi)q^{\xi}+\xi}}} \tag{18} $$

$$ \overline{T}_{1(0,q)} = \frac{1-e^{-q}}{q^2},\ \ and\ \ \overline{T}_{1(y_1,q)} \to 0, as y_1 \to \infty. \tag{19} $$

By some simplifications and using conditions from Eq. (19) into Eq. (18), we get

$$ \overline{T}_{(y,s)} = \frac{1-e^{-q}}{q^2} e^{-y\sqrt{\frac{Pr_1 q^{\xi}a_1}{q^{\xi}+a_2}}} \tag{20} $$

The Laplace inversion of Eq. (20) will be found with a numerical approach in Table 2.

3.2. Solution for velocity equation

By applying the Laplace transform to Eq. (12) with constraints $(9)_1$-$(11)_1$ and the value of temperature from Eq. (20), we obtain

Table 1
The thermophysical characteristics of NPs and base fluid [45].

Material	Water (H_2O)	Copper oxide (CuO)	Aluminum oxide (Al_2O_3)	Titanium Dioxide (TiO_2)
$\rho(M/L^3)$	997.1	6320	3970	425
$C_p(J/MK)$	4179	531.8	765	6862
$k(W/LK)$	0.613	76.5	440	8.9538
$\beta_T(K^{-1})$	21	1.80	0.85	0.9
σ	0.05	0.001	1×10^{-10}	1×10^{-7}

Table 2
Numerical investigation of governed profiles with both numerical techniques.

y	$T_{1(y_1,t_1)}$ by Stehfest	$T_{1(y_1,t_1)}$ by Tzou's	$u_{(y_1,t_1)}$ by Stehfest	$u_{(y_1,t_1)}$ by Tzou's
0.1	0.94104	0.94298	1.0802	1.0811
0.4	0.789	0.79051	1.2525	1.2538
0.7	0.66084	0.66201	1.343	1.3445
1.0	0.55294	0.55385	1.3733	1.3749
1.3	0.46221	0.46292	1.3601	1.3616
1.6	0.38602	0.38657	1.3164	1.3179
1.9	0.3221	0.32253	1.2522	1.2536
2.2	0.26853	0.26887	1.1751	1.1763
2.5	0.22369	0.22395	1.0908	1.0919

$$\overline{u}_{(y_1,q)} = c_3 e^{y_1\sqrt{\frac{1}{\Lambda_1}\left(\frac{q^{\xi}}{(1-\xi)q^{\xi}+\xi}+\beta_1+\Lambda_2 M+\frac{\Lambda_1}{K_2}\right)}} + c_4 e^{-y_1\sqrt{\frac{1}{\Lambda_1}\left(\frac{q^{\xi}}{(1-\xi)q^{\xi}+\xi}+\beta_1+\Lambda_2 M+\frac{\Lambda_1}{K_2}\right)}} - \frac{Gr_1\left(\frac{1-e^{-q}}{q^2}\right)e^{-y\sqrt{\frac{Pr_1 q^{\xi}}{(1-\xi)q^{\xi}+\xi}}}}{\frac{Pr_1 q^{\xi}}{(1-\xi)q^{\xi}+\xi}-\frac{1}{\Lambda_1}\left(\frac{q^{\xi}}{(1-\xi)q^{\xi}+\xi}+\beta_1+\Lambda_2 M+\frac{\Lambda_1}{K_2}\right)} \tag{21}$$

$$\overline{u}_{(0,q)} = G(q), \quad and \quad \overline{u}_{(y_1,q)}\to 0, as y_1\to\infty. \tag{22}$$

Using the boundary conditions from Eq. (22) into Eq. (21), we get the solution of the velocity equation shown below

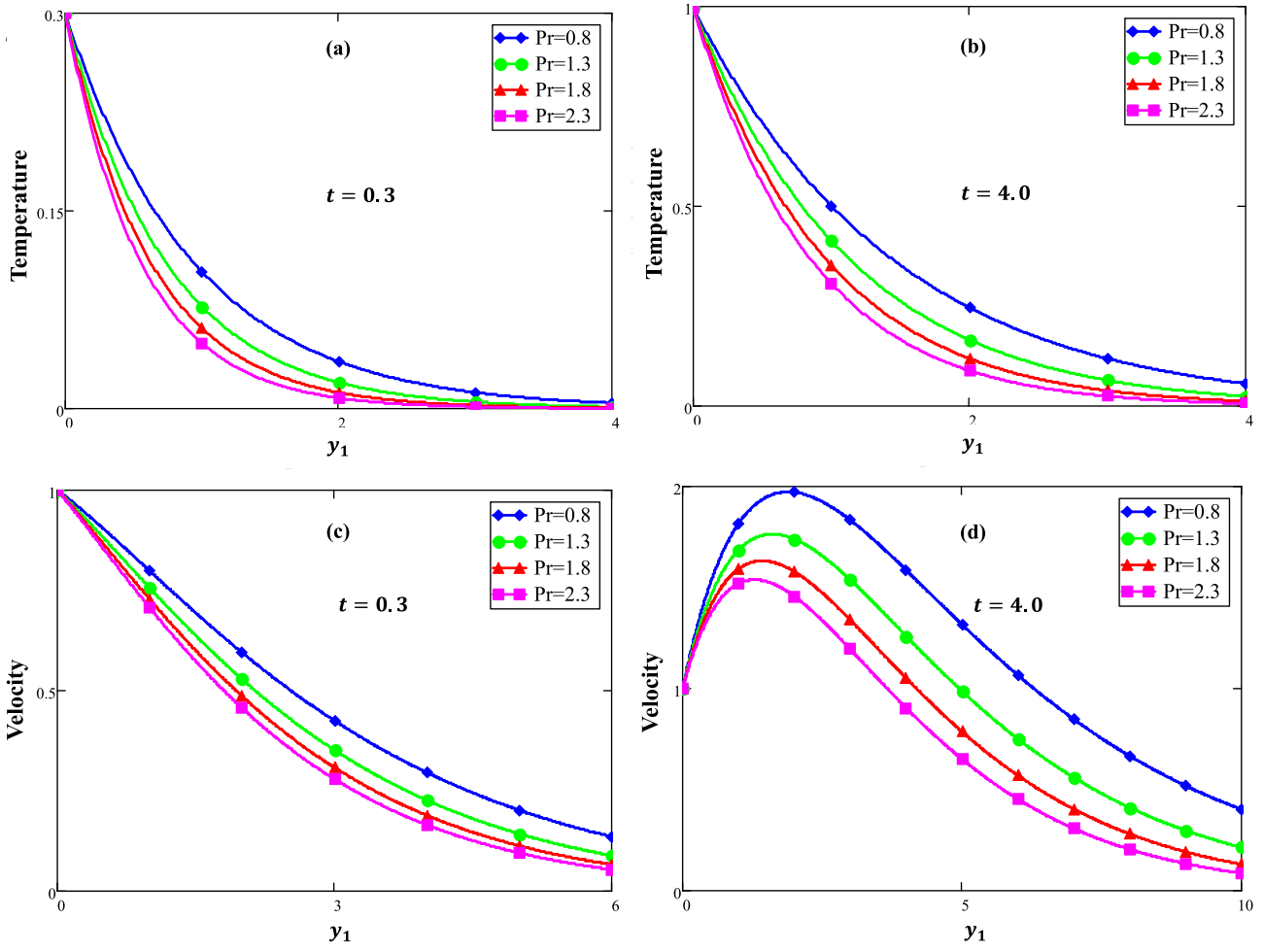

Fig. 4. Significance of Pr on the temperature and velocity profiles when $\phi_1 = \phi_2 = \phi_3 = 0$.

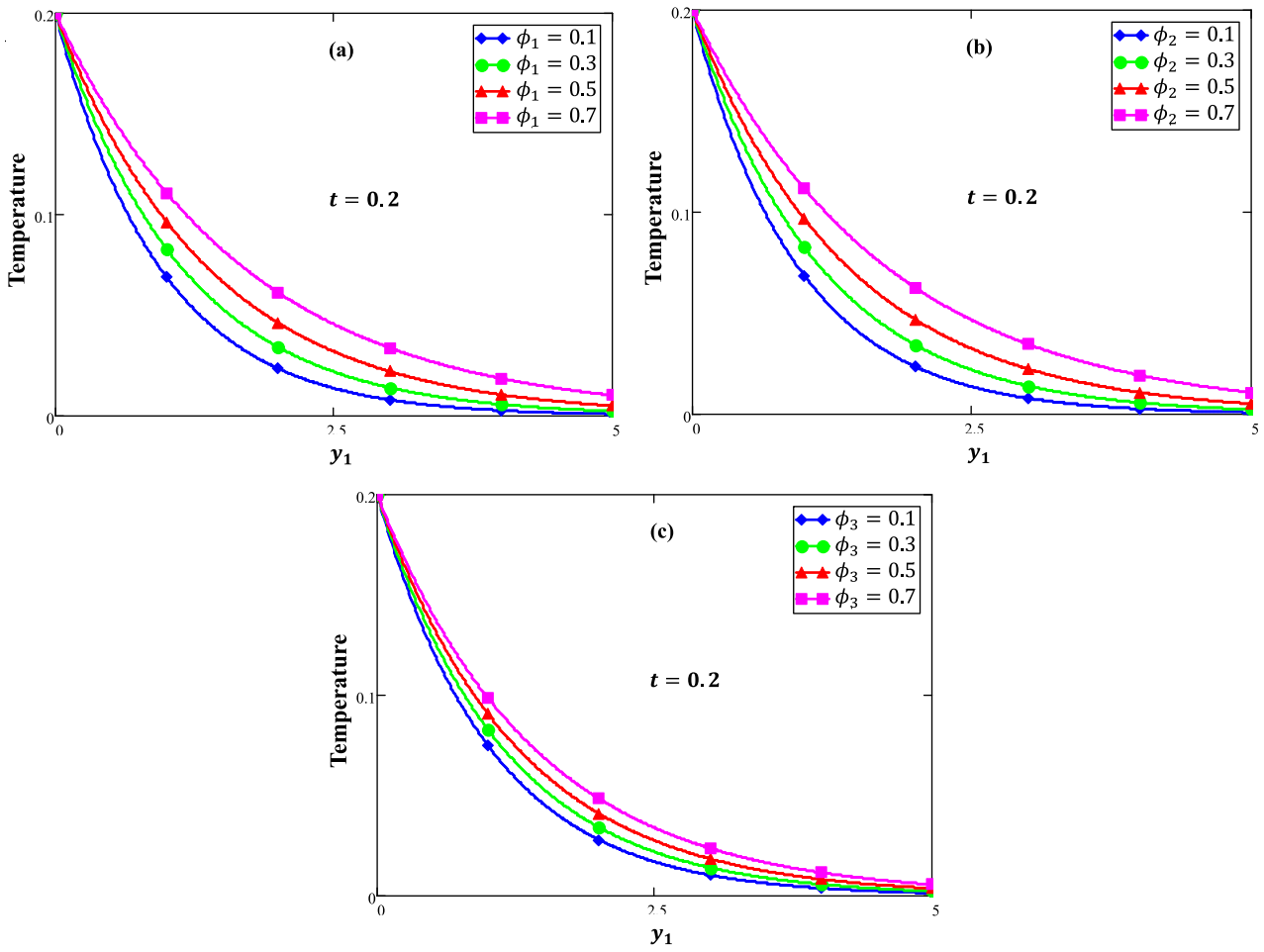

Fig. 5. Significance of Volume fraction ϕ_1, ϕ_2 and ϕ_3 on the temperature field.

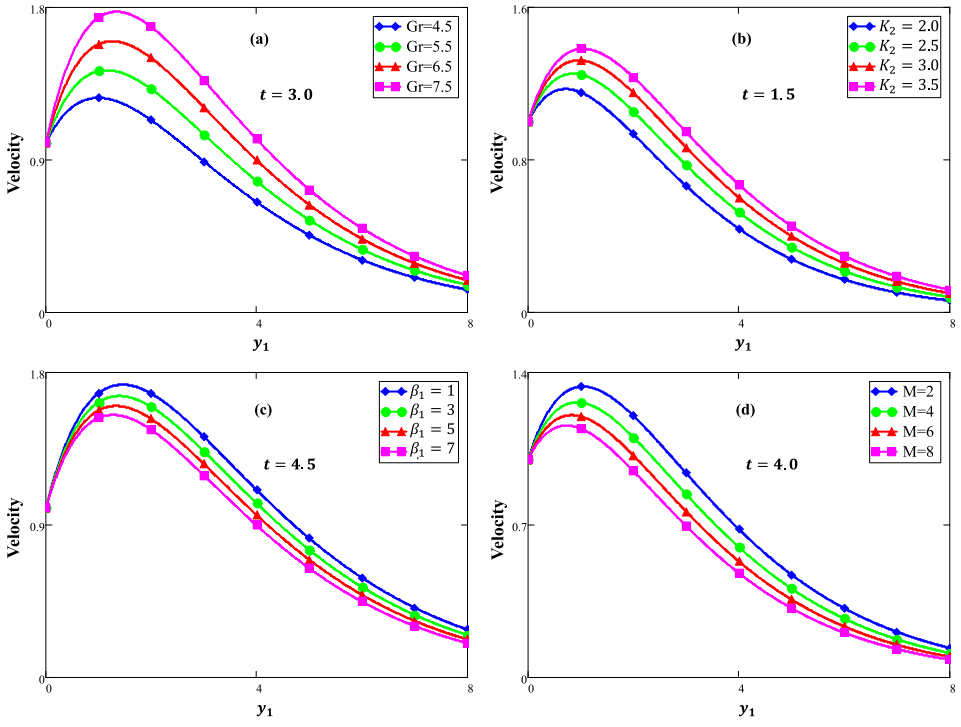

Fig. 6. Significance of Grashof number Gr, permeability parameter K_2, Brinkmann parameter β_1 and magnetic parameter M on the velocity.

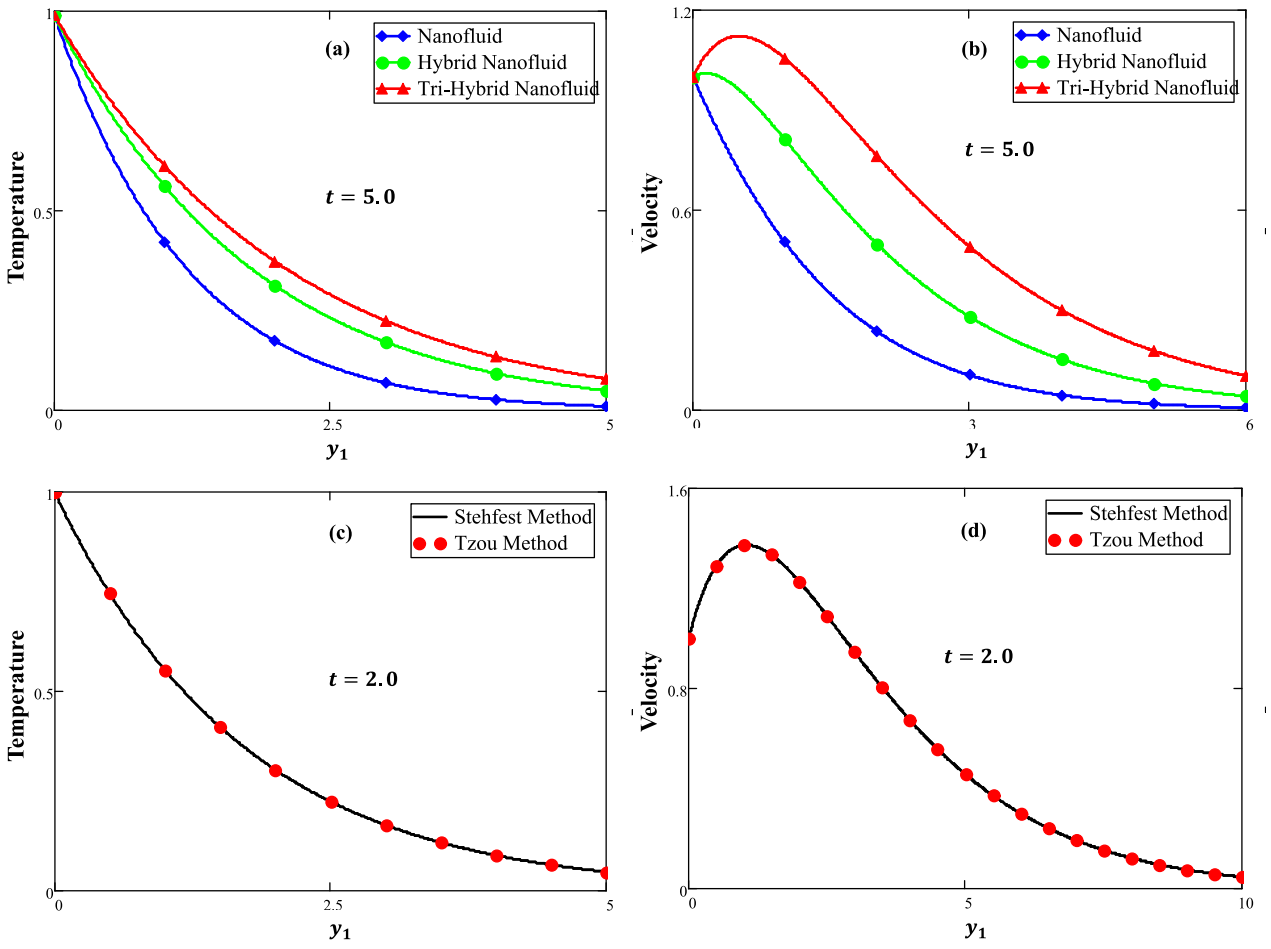

Fig. 7. Comparison of diverse fluids and different numerical methods for temperature and velocity.

$$\overline{u}_{(y_1,q)} = G(q)e^{-y_1\sqrt{\frac{1}{\Lambda_1}\left(\frac{q^{\xi}a_1}{q^{\xi}+a_2}+\beta_1+\Lambda_2 M+\frac{\Lambda_1}{K_2}\right)}} - \left(\frac{1-e^{-q}}{q^2}\right)\frac{Gr_1\Lambda_1(q^{\xi}+a_2)}{q^{\xi}\left(\Lambda_1 Pr_1 a_1 - a_1 - \beta_1 + \Lambda_2 M + \frac{\Lambda_1}{K_2}\right) - a_2\left(\beta_1 + \Lambda_2 M + \frac{\Lambda_1}{K_2}\right)}\left(e^{-y\sqrt{\frac{Pr_1 q^{\xi}a_1}{q^{\xi}+a_2}}} - e^{-y_1\sqrt{\frac{1}{\Lambda_1}\left(\frac{q^{\xi}a_1}{q^{\xi}+a_2}+\beta_1+\Lambda_2 M+\frac{\Lambda_1}{K_2}\right)}}\right) \tag{23}$$

where $a_1 = \frac{1}{1-\xi}$, $a_2 = \xi a_1$.

We have utilized a numerical tool to examine the Laplace inverse of energy and momentum fields by using the Stehfest algorithm. numerically, the Stehfest technique [45] may be illustrated as

$$u(y_1,t_1) = \frac{ln(2)}{t_1}\sum_{m=1}^{M} v_m \overline{u}\left(y_1, m\frac{ln(2)}{t_1}\right)$$

where

$$v_m = (-1)^{m+\frac{M}{2}} \sum_{r=\left[\frac{q+1}{2}\right]}^{min\left(q,\frac{M}{2}\right)} \frac{r^{\frac{M}{2}}(2r)!}{\left(\frac{M}{2}-r\right)!r!(r-1)!(q-r)!(2r-q)!}$$

We also applied the Tzou scheme [46], which is considered to be rigorous theoretically, to compare and validate the results obtained by the previous numerical methods.

$$u(y_1,t_1) = \frac{e^{4.7}}{t_1}\left[\frac{1}{2}\overline{u}\left(y_1,\frac{4.7}{t_1}\right) + Re\left\{\sum_{k=1}^{M}(-1)^k \overline{u}\left(y_1,\frac{4.7+k\pi i}{t_1}\right)\right\}\right]$$

Table 3
Numerical study of Nusselt number and skin friction.

α	Nu	C_f
0.1	0.333	0.36549
0.2	0.3383	0.36938
0.3	0.34706	0.37552
0.4	0.35952	0.38386
0.5	0.37616	0.39457
0.6	0.39778	0.40806
0.7	0.42545	0.425
0.8	0.46006	0.44623
0.9	0.49914	0.47054

Table 4
Numerical analysis of governed profiles comparison of nanofluid and tri-hybrid nanofluid.

	Temperature Profile			Velocity Profile		
y	Nanofluid	Tri-hybrid nanofluid	% age increase	Nanofluid	Tri-hybrid nanofluid	% age increase
0.3	0.7593	0.8579	13	0.7989	1.0798	35
0.6	0.5698	0.729	28	0.6289	1.0688	70
0.9	0.4263	0.6188	45	0.49	1.0068	105
1.2	0.3181	0.5247	65	0.3789	0.9188	142
1.5	0.2366	0.4445	88	0.2913	0.8205	182
1.8	0.1756	0.3762	114	0.2227	0.7215	224
2.1	0.13	0.3181	145	0.1696	0.6271	270
2.4	0.096	0.2687	180	0.1286	0.5402	320
2.7	0.0708	0.2268	220	0.0971	0.4621	376
3.0	0.052	0.1913	268	0.0731	0.3931	438

3.3. Gradients

In this section, the following two substantial engineering quantities of consideration are hired the Nusselt number and the skin friction coefficient. These gradients are specified as:

$$Nu = -\left.\frac{\partial T_{(y_1,t_1)}}{\partial y_1}\right|_{y_1=0} = -\mathscr{L}^{-1}\left\{\frac{\partial \overline{T}_{(0,q)}}{\partial y_1}\right\}, \tag{24}$$

$$C_f = -\left.\frac{\partial u_{(y_1,t_1)}}{\partial y_1}\right|_{y_1=0} = -\mathscr{L}^{-1}\left\{\frac{\partial \overline{u}_{(0,q)}}{\partial y_1}\right\}. \tag{25}$$

4. Discussion of results

This section is devotedly detailed to the substantial character of nanoparticles (copper oxide, aluminum oxide, and titanium oxide) and of water as base fluid. Here, tri-hybrid NF is exhibited via the newly introduced definition of fractional differentiations, namely as AB-fractional derivative and the mathematical models of temperature as well as velocity are solved with Laplace transforms. The results stated below for thermal transmission and momentum profile have taken a comparative investigation of tri-hybrid NF. The implications of fractional and diverse involved flow parameters on temperature and momentum are shown in Figs. 3-7 for the small as well as significant times. The thermophysical characteristics of used nanoparticles have been taken from Table 1 for graphical demonstration.

Fig. 3 is anticipated to display the influence of the fractional parameters ξ on temperature and momentum profiles. For a small value of time, temperature and momentum fields are declined by increasing ξ. This is due to the boundary layer expanding; as a result, temperature and velocity decrease, and behaviors are reversed for high values of time. Generally, a fractional technique is preferable in fluid dynamics for controlling the fluid's boundary layer viscosity. Fig. 4 is projected to display the impact of the Pr when $\phi_1 = \phi_2 = \phi_3 = 0$ on temperature, as well as velocity. Physically, when Pr values rise, temperature boundary layer viscosity falls rapidly, causing decay in both the energy and velocity profiles. Fig. 5 shows that temperature rises with the growth in ϕ_1, ϕ_2 and ϕ_3. This is due to the temperature conductivity growing with the enhancement of ϕ_1, ϕ_2 and ϕ_3, and the fluid presentation more temperature so, of heat transmission rises, which hints at an intensification in the momentum profile.

Fig. 6 is depicted to demonstrate the influences of Grashof number Gr, permeability parameter K_2, Brinkmann parameter β_1 and magnetic parameter M on the velocity. Fig. 6(a) illustrates the impacts of Gr on velocity. A rise in Gr is thought to increase momentum due to an increase in buoyant force caused by temperature gradients. Gr denotes the effect of thermal buoyancy forces on the viscid hydrodynamic force. Growing Gr indicates a growth in temperature gradients, which causes the role of buoyancy near to the plate to become more significant, resulting in a temporary increase in speed close to the plate. Fig. 6(b) exhibits the impact of K_2 on the velocity. It is detected that a higher estimation of K_2 enlarging the momentum field. This is the reason for the drop in resistance of the porous medium and the reasons development of the viscosity of the velocity boundary layer. The significance of the Brinkman parameter on the momentum is exposed in Fig. 6(c). Velocity lessened as the Brinkman parameter was enlarged. This is because increasing the Brinkman parameter increases the drag forces, causing speed to decrease.

The effect of magnetic parameter M on the velocity is perceived in Fig. 6(d). It can be detected that the fluid movement is retarded, and the velocity profile declined for an enormous value of the magnetic field. Because the magnetic field plays a role in the increase in the Lorentz force, at advanced levels of M, the resistance grows and tends to impede the fluid flow, considerably reducing the fluid speed. Fig. 7 is depicted to demonstrate the comparison of various fluids and different numerical methods on the temperature as well as on velocity. Fig. 7(a, b) exhibits the impacts of NF, HNF, and tri-HNF on both profiles. It is well-known that as constituents of alike features are collective, the combined effect is enhanced for different volumes of the mixture. It can be observed that the influence of tri-hybrid nanofluid dominates the impact of hybrid nanofluid, which overlooks the effect of simple nanofluid. Thus, temperature and velocity profiles are improved by varying the number of nanoparticles (see Table 3 and Table 4).

An equivalence relation is chosen in Fig. 7(c, d) as well as in Table 1 to see the validity of the consequences with the numerical inversion of Laplace transforms explicitly. Stehfest, as well as Tzou techniques for temperature and velocity. Table 1 displays the estimations of two diverse systems, i.e., Stehfest and Tzou, to obtain the inverse Laplace for the temperature and velocity solution. Mathematically, it is evident that the results derived from these two disparate procedures are highly approximated to one other.

5. Conclusions

An innovative fractionalized model because of tri-hybrid NF is deliberated and examined using a non-local kernel. The fractional model of tri-hybrid NF is handled by employing recently presented definitions of fractional approaches known as AB-time fractional derivative. The Laplace transform is operated on the governing equations of energy and velocity with tri-hybrid NF. The semi-analytical solution of the fractional governing equations of tri-hybrid NF is obtained. The following results are emphasized:

- Velocity and temperature exposed dual behavior for ξ for a short and large time. This might be related to the kernel of the fractional

differential operator, which explains the function's memory for fluid behavior.

- Enhancing the estimations of the volume fraction of nanoparticles ϕ_1, ϕ_2 and ϕ_3, consequently enhancing the temperature.
- By increasing *Pr*, the temperature and velocity profiles are reduced due to decrement in the boundary layer.
- In compared to other fractional models, the AB-fractional derivative has better memory significance.
- Increasing the value of *Gr* leads to growing momentum. This causes the role of buoyancy near the plate to become more significant, resulting in increased speed close to the plate.
- The momentum profile declined with a rise in Brinkman-type fluid parameter β_1 due to increases in the drag forces
- Velocity rises with the rising values of the permeability parameter K_2.
- Temperature, as well as velocity, exhibited higher profiles for tri-hybrid NF as compared to hybrid NF or simply NF.
- The overlapping of both curves of numerical schemes represents the validation of attained results.

Declaration of Competing Interest

The authors declare that they have no known competing financial interests or personal relationships that could have appeared to influence the work reported in this paper.

References

[1] Choi SU, Eastman JA. Enhancing thermal conductivity of fluids with nanoparticles (No. ANL/MSD/CP-84938; CONF-951135-29). Argonne National Lab.(ANL), Argonne, IL (United States); 1995.
[2] Ellahi R, Hassan M, Zeeshan A, Khan AA. The shape effects of nanoparticles suspended in HFE-7100 over wedge with entropy generation and mixed convection. Appl Nanosci 2016;6(5):641–51.
[3] Meften GA, Ali AH. Continuous dependence for double diffusive convection in a Brinkman model with variable viscosity. Acta Universitatis Sapientiae. Mathematica 2022;14(1):125–46.
[4] Ali AH, Meften GA, Bazighifan O, Iqbal M, Elaskar S, Awrejcewicz J. A study of continuous dependence and symmetric properties of double diffusive convection: forchheimer model. Symmetry 2022;14(4):682.
[5] Gourari S, Mebarek-Oudina F, Hussein AK, Kolsi L, Hassen W, Younis O. Numerical study of natural convection between two coaxial inclined cylinders. Int J Heat Technol 2019;37(3):779–86.
[6] Mebarek-Oudina F. Convective heat transfer of Titania nanofluids of different base fluids in cylindrical annulus with discrete heat source. Heat Trans—Asian Res 2019;48(1):135–47.
[7] Raza J, Mebarek-Oudina F, Chamkha AJ. Magnetohydrodynamic flow of molybdenum disulfide nanofluid in a channel with shape effects. Multidiscip Model Mater Struct 2019.
[8] Alfvén H. Existence of electromagnetic-hydrodynamic waves. Nature 1942;150 (3805):405–6.
[9] Aly EH, Pop I. MHD flow and heat transfer over a permeable stretching/shrinking sheet in a hybrid nanofluid with a convective boundary condition. Int J Numer Meth Heat Fluid Flow 2019.
[10] Chamkha AJ, Dogonchi AS, Ganji DD. Magnetohydrodynamic nanofluid natural convection in a cavity under thermal radiation and shape factor of nanoparticles impacts: a numerical study using CVFEM. Appl Sci 2018;8(12):2396.
[11] Dogonchi AS, Ganji DD. Investigation of heat transfer for cooling turbine disks with a non-Newtonian fluid flow using DRA. Case Stud Therm Eng 2015;6:40–51.
[12] Veera Krishna M. Heat transport on steady MHD flow of copper and alumina nanofluids past a stretching porous surface. Heat Transfer 2020;49(3):1374–85.
[13] Ramadhan AI, Azmi WH, Mamat R. Stability and thermal conductivity of tri-hybrid nanofluids for high concentration in water-ethylene glycol (60: 40). Nanosci Nanotechnol-Asia 2021;11(4):121–31.
[14] Muzaidi NAS, Fikri MA, Wong KNSWS, Sofi AZM, Mamat R, Adenam NM, et al. Heat absorption properties of CuO/TiO2/SiO2 trihybrid nanofluids and its potential future direction towards solar thermal applications. Arab J Chem 2021; 14(4):103059.
[15] Gul T, Saeed A. Nonlinear mixed convection couple stress tri-hybrid nanofluids flow in a Darcy-Forchheimer porous medium over a nonlinear stretching surface. Waves Random Complex Media 2022:1–18.
[16] Adun H, Kavaz D, Dagbasi M. Review of ternary hybrid nanofluid: Synthesis, stability, thermophysical properties, heat transfer applications, and environmental effects. J Clean Prod 2021;328:129525.
[17] Rauf A, Faisal Shah NA, Botmart T. Hall current and morphological effects on MHD micropolar non-Newtonian tri-hybrid nanofluid flow between two parallel surfaces. Sci Reports 2022; 12(1): 16608.
[18] Sahu M, Sarkar J, Chandra L. Steady-state and transient hydrothermal analyses of single-phase natural circulation loop using water-based tri-hybrid nanofluids. AIChE J 2021;67(6):e17179.
[19] Xuan Z, Zhai Y, Ma M, Li Y, Wang H. Thermo-economic performance and sensitivity analysis of ternary hybrid nanofluids. J Mol Liq 2021;323:114889.
[20] Devi SA, Devi SSU. Numerical investigation of hydromagnetic hybrid Cu–Al2O3/ water nanofluid flow over a permeable stretching sheet with suction. Int J Nonlinear Sci Numer Simul 2016;17(5):249–57.
[21] Krishna MV, Ahammad NA, Chamkha AJ. Radiative MHD flow of Casson hybrid nanofluid over an infinite exponentially accelerated vertical porous surface. Case Stud Therm Eng 2021;27:101229.
[22] Dupret F, Couniot A, Mal O, Vanderschuren L, Verhoyen O. Modelling and simulation of injection molding, rheology series; 1999.
[23] Peng Y, Lv BH, Yuan JL, Ji HB, Sun L, Dong CC. Application and prospect of the non-Newtonian fluid in industrial field. In: Materials Science Forum, Vol. 770. Trans Tech Publications Ltd; 2014, pp. 396-401.
[24] Wu WT, Massoudi M. Recent advances in mechanics of Non-Newtonian fluids. Fluids 2020;5(1):10.
[25] Darcy H. Les fontaines publiques de la ville de Dijon: Exposition et application des principes à suivre et des formules à employer dans les questions de distribution d'eau: Ouvrage terminé par un appendice relatif aux fournitures d'eau de plusieurs villes, au filtrage des eaux et à la fabrication des tuyaux de fonte, de plomb, de tôle et de bitume (Vol. 2). V. Dalmont; 1856.
[26] Brinkman HC. On the permeability of media consisting of closely packed porous particles. Flow Turbul Combust 1949;1(1):81–6.
[27] Brinkman HC. The viscosity of concentrated suspensions and solutions. J Chem Phys 1952;20(4):571.
[28] Abed Meften G, Ali AH, Al-Ghafri KS, Awrejcewicz J, Bazighifan O. Nonlinear stability and linear instability of double-diffusive convection in a rotating with LTNE effects and symmetric properties: brinkmann-forchheimer model. Symmetry 2022;14(3):565.
[29] Gorla RSR, Mansour MA, Sahar MG. Natural convection from a vertical plate in a porous medium using Brinkman's model. Transp Porous Media 1999;36(3): 357–71.
[30] Lin C, Payne LE. Structural stability for a Brinkman fluid. Math Methods Appl Sci 2007;30(5):567–78.
[31] Abro KA, Khan I, Gomez-Aguilar JF. A mathematical analysis of a circular pipe in rate type fluid via Hankel transform. Eur Phys J Plus 2018;133(10):397.27.
[32] Ying Y, Lian Y, Tang S, Liu WK. High-order central difference scheme for Caputo fractional derivative. Comput Methods Appl Mech Eng 2017;317:42–54.
[33] Abro KA, Yıldırım A. Fractional treatment of vibration equation through modern analogy of fractional differentiations using integral transforms. Iranian J Sci Technol, Trans A: Sci 2019;43(5):2307–14.
[34] Ali Q, Riaz S, Awan AU, Abro KA. A mathematical model for thermography on viscous fluid based on damped thermal flux. Zeitschrift für Naturforschung A 2021; 76(3):285–94.
[35] Li D, Zuo W, Li Q, Zhang G, Zhou K, Jiaqiang E. Effects of pulsating flow on the performance of multi-channel cold plate for thermal management of lithium-ion battery pack. Energy 2023;273:127250.
[36] Zuo W, Wang Z, Jiaqiang E, Li Q, Cheng Q, Wu Y, et al. Numerical investigations on the performance of a hydrogen-fueled micro planar combustor with tube outlet for thermophotovoltaic applications. Energy 2023;263:125957.
[37] Zuo W, Chen Z, Jiaqiang E, Li Q, Zhang G, Huang Y. Effects of structure parameters of tube outlet on the performance of a hydrogen-fueled micro planar combustor for thermophotovoltaic applications. Energy 2023;266:126434.
[38] Zuo W, Zhang Y, Jiaqiang E, Li J, Li Q, Zhang G. Performance comparison between single S-channel and double S-channel cold plate for thermal management of a prismatic LiFePO4 battery. Renew Energy 2022;192:46–57.
[39] Khan ZA, Haq SU, Khan TS, Khan I, Tlili I. Unsteady MHD flow of a Brinkman type fluid between two side walls perpendicular to an infinite plate. Results Phys 2018; 9:1602–8.
[40] Zhang J, Raza A, Khan U, Ali Q, Zaib A, Weera W, et al. Thermophysical Study of Oldroyd-B Hybrid Nanofluid with Sinusoidal Conditions and Permeability: A Prabhakar Fractional Approach. Fractal Fractional 2022;6(7):357.
[41] Ali Q, Al-Khaled K, Omar J, Raza A, Khan SU, Khan MI, et al. Analysis for advection–diffusion problem subject to memory effects and local and nonlocal kernels: A fractional operators approach. Int J Mod Phys B 2022:2350099.
[42] Ullah Khan S, Raza A, Prasannakumara BC, Reddy YD, Khan MI. Inspecting heat transport phenomenon in the flow of non-Newtonian fluid in the presence of Newtonian heating and inclined slip: fractional derivative framework. Waves Random Complex Media 2023:1–12.
[43] Raza A, Al-Khaled K, Khan SU, Elboughdiri N, Farah A, Gasmi H, et al. Progressive thermal onset of modified hybrid nanoparticles for oscillating flow via modified fractional approach. Int J Mod Phys B 2023;37(05):2350046.

[44] Raza A, Khan SU, Farid S, Khan MI, Sun TC, Abbasi A, et al. Thermal activity of conventional Casson nanoparticles with ramped temperature due to an infinite vertical plate via fractional derivative approach. Case Stud Therm Eng 2021;27:101191.
[45] Ghara N, Das S, Maji SL, Jana RN. Effect of radiation on MHD free convection flow past an impulsively moving vertical plate with ramped wall temperature. Am J Sci Ind Res 2012;3(6):376–86.
[46] Tzou DY. Macro-to microscale heat transfer: the lagging behavior. John Wiley & Sons; 2014.

Ali Hasan Ali is a dedicated researcher at the Institute of Mathematics, University of Debrecen, Hungary. He holds a B. Sc. Ed. in Mathematics from University of Mosul, Iraq, and an M.Sc. in Applied Mathematics from Wright State University, USA, and a Ph.D. in Mathematics from University of Debrecen, Hungary. Ali's research interests include Applied Mathematics, Modelling, Optimization, Fractional Calculus, Computational Mathematics, and Approximation. He has published over 50 research papers in Scopus/WOS-indexed journals in esteemed publishers, including Elsevier, Springer, Wiley, Taylor and Francis, and IEEE. In addition to his research, Ali actively contributes to the academic community as a reviewer for prestigious journals and has served as the Program Committee Chair and member for numerous international conferences.